Available online at www.sciencedirect.com

ScienceDirect

Physics Procedia 83 (2016) 778 – 788

Physics Procedia

9th International Conference on Photonic Technologies - LANE 2016

Deformation behavior and microstructure of Ti6Al4V manufactured by SLM

P. Krakhmalev[a,*], G. Fredriksson[a], I. Yadroitsava[b], N. Kazantseva[c], A. du Plessis[d], I. Yadroitsev[b]

[a]*Karlstad University, Department of Engineering and Physics, Karlstad SE-651 88, Sweden*
[b]*Central University of Technology, Free State, Department of Mechanical and Mechatronic Engineering, Private Bag X20539, Bloemfontein 9300, South Africa*
[c]*Institute of Metal Physics, Urals Branch of the Academy of Sciences, Ekaterinburg 620219, Russia*
[d]*University of Stellenbosch, CT Scanner Facility, Private Bag X1, Matieland, Stellenbosch 7602, South Africa*

- Invited Paper -

Abstract

Mechanical properties, porosity, and microstructure of Ti6Al4V (ELI) material produced by Selective Laser Melting (SLM) under controlled oxygen content were analyzed. Fully martensitic α′structure with high dislocation density and stacking faults was observed in both as-built and stress relieved samples by means of XRD and TEM. Tensile $\{10\bar{1}2\}$ twinning was identified by TEM and electron diffraction. Accommodation of thermal stresses during manufacturing was suggested as a possible reason for twinning. Computed tomography of pores was carried out. Pores in the specimens were evenly distributed and mostly had an elongated shape. Defect analysis by micro CT scans in pre-strained samples confirmed that the pore coalescence was the main crack formation mechanism in the final fracture with typical cup-and-cone fracture morphology. Additionally, typical dimples and quasi-cleavage were revealed. Mechanical properties of the samples after stress relieving heat treatment at 650°C for 3 h are complied with the international standard for Ti alloys for biomedical applications.

Peer-review under responsibility of the Bayerisches Laserzentrum GmbH

Keywords: Ti6Al4V; tensile test; mechanical properties; porosity; microstructure; twinning

* Corresponding author. Tel.: +46-547002036 .
E-mail address: Pavel.Krakhmalev@kau.se

Peer-review under responsibility of the Bayerisches Laserzentrum GmbH
doi:10.1016/j.phpro.2016.08.080

1. Introduction

Modern implants are produced from titanium alloys, stainless-steel, cobalt-chromium alloys and noble metals. Implants from titanium alloys have many benefits: high strength, good fracture toughness, high corrosion resistance and low weight. They are non-ferromagnetic, cost-efficient, non-toxic, biocompatible, long-lasting, and have capacity for osseointegration. It should be noted that according to the standard specifications for wrought Ti6Al4V (ELI) and cast Ti6AlV alloys for surgical implant applications (ASTM F136-13 and ASTM F1108-14), the elongation of the material should be at least 8%.

The mechanical properties of conventional two-phase titanium alloys, like Ti6Al4V, strongly depend on the amount, distribution and morphology of the phases (Donachie, 2000). Equiaxed microstructures, consisting of globular fine-grained α-phase dispersed in a β-phase matrix, have superplastic characteristics and provide an optimum combination of strength, ductility and fatigue resistance (Boyer et al., 1994). Ti6Al4V with lamellar structures has high strength with some decrease in ductility and demonstrates good fracture toughness. Refinement of the microstructure results in a higher yield stress. However, as it has been shown by Sieniawski et al. (2013), the increase of yield stress is moderate unless a martensitic phase is present. Content of interstitials also has substantial influence on ductility and strength of Ti6Al4V. As it has been indicated by Boyer et al. (1994) and Donachie (2000), an oxygen content higher than 0.2 wt.% leads to an increase in strength and a remarkable decrease in ductility of Ti6Al4V alloy. Decrease in oxygen and nitrogen content improves the ductility, fracture toughness, stress-corrosion resistance and resistance against crack growth.

Selective laser melting (SLM) provides an excellent opportunity to manufacture custom implants of complex shapes with the desired inner structure and surface morphology. Microstructure of SLM Ti6Al4V is formed at direct rapid solidification and β to α′ (alpha prime) transformation at very high cooling rates (about 10^6 K/s). This state is far away from the conventional plastically deformed and heat treated material. High cooling rates at SLM result in a formation of the acicular/lamellar α′ hexagonal martensitic phase. This microstructure is inherently less ductile than the globular microstructure formed during conventional processing (Kasperovich et al., 2015). Analysis of the literature shows that although basic mechanical properties have been reported many times, there is a substantial deviation in mechanical property data. In the as-built SLM sample, the structure consists of many tracks and layers having metallurgical contact with each other. Therefore, the mechanical properties depend on the manufacturing strategy, the initial powder, energy input, layer thickness and other parameters.

Due to high cooling rates, tensile residual stresses generated during SLM detrimentally affect the mechanical behavior of the parts, (Yadroitsava et al., 2015) and (Vrancken et al., 2012). To minimize any possible distortion, SLM objects are subjected to stress relieving heat treatment before separation from the substrate. For conventional Ti6Al4V, further heat treatments are usually used to change the microstructure and optimize the mechanical properties. For SLM Ti6Al4V, after many attempts, it has been found challenging to apply heat treatment regimes used for conventional materials directly. This is because the SLM materials have different structure and metallurgical history (Vrancken et al., 2012).

A possibility to use SLM Ti6Al4V after manufacturing and stress relieve (if requirements to ductility are fulfilled) would therefore be advantageous. Thus, deeper understanding of the microstructure and mechanisms governing the mechanical performance of the material in the as-built and stress relieved conditions is necessary. This investigation is dedicated to characterization of microstructure, porosity and properties of SLM Ti6Al4V in as-built and stress relieved conditions. A special focus was paid on porosity and its development after pre-tension to explain the observed failure mechanisms. Deeper understandings of microstructural changes after stress relieve, in situ twinning and its influence on mechanical properties is presented. The new knowledge on microstructure-properties-heat treatment relationship is important to find possible industrial applications of SLM Ti6Al4V after stress relief treatment, and necessary for the future development of new regimes of heat treatments of SLM Ti6Al4V.

2. Materials and method

Ti6Al4V (Extra Low Interstitial alloy, ELI) powder was provided by TLS Technik GmbH. According to the manufacturing specification, the particle size was d_{10}:11.16 μm, d_{50}:20.64 μm, d_{90}:31.84 μm (weighted by volume).

The powder had a spherical morphology, typical for gas atomization process. Before manufacturing, the powder was dried at 80°C for 2 hours.

Horizontal samples were produced by the EOSINT M280 machine (EOS GmbH) equipped with an Ytterbium fiber laser operating at 1075 nm wavelength (IPG Photonics Corp.). The laser beam had a TEM00 Gaussian profile and 80 μm spot diameter. In accordance with standard process parameters for a Ti6Al4V alloy, a powder layer thickness of 30 μm, and a back-and-forth (zig-zag) scanning by strips with the hatch distance of 100 μm was applied. The substrate and powder material was similar in chemical composition. Argon was used as the protective atmosphere; the oxygen level in the chamber was 0.07–0.12%.

Scanning electron microscopy (SEM) was carried out with LEO 1350 FEG-SEM and analytical SEM Hitachi SU70, both operated at 20 kV. Transmission electron microscopy (TEM) was done with JEOL JEM 2100, equipped with a LaB_6 cathode, and JEM-200CX.

Round metal specimens with threaded ends were machined from SLM rectangular bars with 10 mm in height, 10 mm – width and length of 60 mm according to ASTM E8M (gauge length four times the diameter, Specimen 4). Tensile tests were performed with an Instron 1342 servo-hydraulic testing machine with clip-on extensometer under constant strain rate of 1.5 mm/min.

Heat treatment for stress relieving was done in Ar atmosphere at 650°C for 3 hours. Samples were subjected to X-ray micro computed tomography (MicroCT), before and after stress relieving and tensile tests. Due to the potential for improved image contrast, the MicroCT scans were done at 10 μm resolution. MicroCT scans were done with a General Electric Phoenix V|Tome|X L240 system at 160 kV and 200 μA. All analyses reported here were done with Volume Graphics VGStudioMax 2.2 including the defect analysis module and the nominal/actual comparison module. 3D image processing was done using selection and morphological image operations to select the sample sub-surface by 5 voxels, in order to eliminate any edge noise effects. Therefore any voids touching the sample edge would not be included in the analysis up to 5 voxels (50 μm).

3. Results and discussion

3.1. Mechanical properties and porosity

Table 1 summarizes results on mechanical properties of SLM Ti6Al4V specimens manufactured in horizontal orientation. For Ti6Al4V alloy, data obtained in the present investigation and literature data are in a good agreement, although some deviation was observed. The ultimate tensile strength (UTS), published in the literature, varied from 1140 to 1407 MPa and the average yield strength (YS) from 990 to 1333 MPa. A comparison of results of tensile mechanical properties showed that different laser power densities (the ratio of laser power to spot area) from 5 to 118 kW/mm^2, different scanning speeds and scanning strategies lead to quite similar YS and UTS characteristics, of SLM Ti6Al4V ELI with/without preheating, Table 1.

Accordingly to standards for medical applications, ductility properties also have to be high and the reduction in area must be 14-15 % or higher, and elongation higher than 8% (ASTM F136-13 and ASTM F1108-14). Generally, a deviation among the measured elongation results is quite significant, Table 1. The experimentally observed in this study values of area reduction were 25.6±2.41 % for as-built and 29.3±2.66 % in stress relieved specimen. The average measured elongation was 9.4±0.42 % for as-built and 10.9±0.75 % for SLM Ti6Al4V ELI after stress relief. These values are quite high compared to the other results summarized in Table 1.

It has been shown that the ductility of Ti6Al4V is very sensitive to interstitial content (Miura et al., 2010). Ductility of PM Ti6Al4V samples reduced dramatically at oxygen contents greater than 0.35 wt.%, as shown by Xu et al., (2015). In the present investigations, manufacturing under controlled oxygen content was done. 0.19 wt.% oxygen and 0.058 wt.% nitrogen were measured in the investigated specimens, which is slightly higher than the nominal content of interstitials in the powder. The deviation in ductility data presented in Table 1 could be a result of different content of interstitials in the specimens.

Porosity also has a crucial impact on the final material properties and performance. For samples manufactured in horizontal direction, the tension load is applied perpendicularly to the building direction. Then, a lack of fusion between tracks and/or stripes and/or islands can be critical in terms of ductility.

Recently, a computed tomography method was efficiently used for analysis of porosity in SLM 316 stainless steel (Ziolkowski et al., 2014), SLM Ti6Al4V (S. Tammas-Williams et al., 2015), cast Ti6Al4V (du Plessis et al., 2015), and aluminum alloy (I. Maskery et al., 2016). Nevertheless, to carry out a systematic analysis of influence of selective laser melting parameters on porosity characteristics, more experimental data is required.

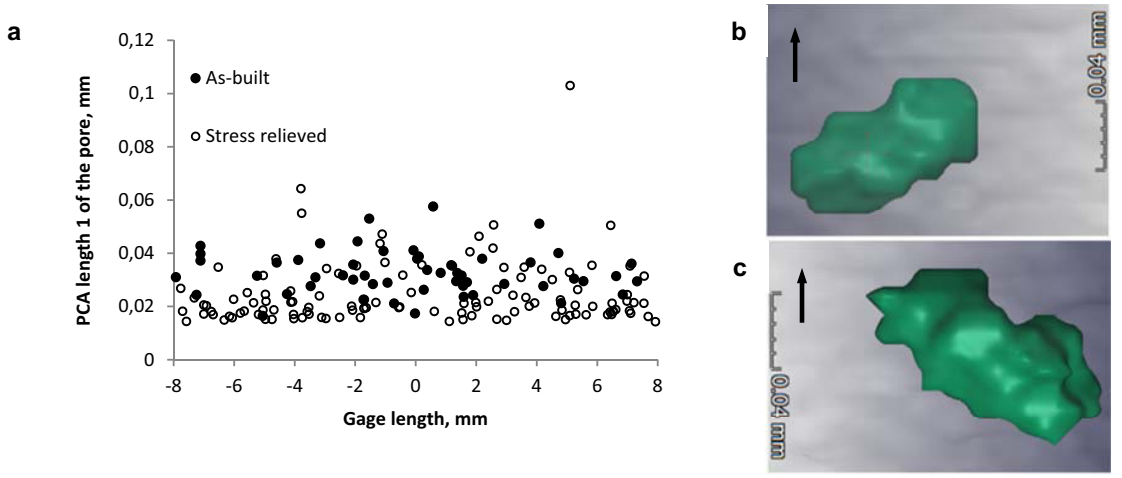

Fig. 1. (a) PCA length of the pores in as-built and stress relieved samples, (b) graphical reconstruction of the typical pores in as-built and (c) in stress relieved samples. Arrow corresponds to building direction.

Table 1. Mechanical properties of Ti6Al4V samples produced by SLM*.

	Density, %	UTS, MPa	YS, MPa	E, GPa	ε_f, %
Ti6Al4V alloy					
Facchini et al. (2010)		1140±10	1040±10		8.2±0.3
Facchini et al. (2010)	99.7±0.1	1095±10	990±5	110±5	8.1±0.3
Frey et al. (2009)		1248	1043	112	8.5
Rafi et al. (2013)		1269±9	1195±19		5±0.5
Murr et al. (2009)		1407	1333		4.54
Mertens et al. (2014) Along/Across Ar flow	99.5	1321±6 / 1214±24	1166±6 / 1140±43	112	2±0.7 / 3.2±2
Cast, HIP and annealed Ti6Al4V ASTM F1108-14		Min 860	Min 758		Min 8
Ti6Al4V (ELI)					
Vrancken et al. (2012)	>99.9	1267±5	1110±9	109.2±3.1	7.28±1.12
Vilaro et al. (2011)	>99	1206±8	1137±20	105±5	7.6±2
Present as-built	>99.9	1265±4.8	1098±2	112±2.1	9.4±0.42
Present stress relieved		1170±5.7#	1098±4.8	117±2.2#	10.9±0.75#
Annealed wrought Ti6Al4V (ELI) ASTM F136-13		Min 825	Min 760		Min 8

*Tensile properties for horizontal as-built material; for present study data is indicated for as-built and stress relieved samples

Significant differences (*t-test, $p<0.05$*)

All samples investigated in present work were produced to minimize porosity, i.e. with optimal process-parameters. The MicroCT scans analysis carried out in this investigation showed that as-built SLM and stress relieved samples both had low levels of porosity; the estimated porosities were 0.0018% and 0.0022% respectively.

Totally 53 pores were detected in the as-built specimen, and 120 pores were observed in the stress relieved one, although the total pore volume was found similar in both. The pores were randomly distributed throughout the samples. The biggest detected pore was found in the stress relieved sample and had a PCA (Principal Component Analysis) length of 104 μm. Most pores had an elongated shape, the average elongation for the as-built sample was 1.6±0.25 μm and 1.7±0.37 μm for the stress relieved one, Fig. 1.

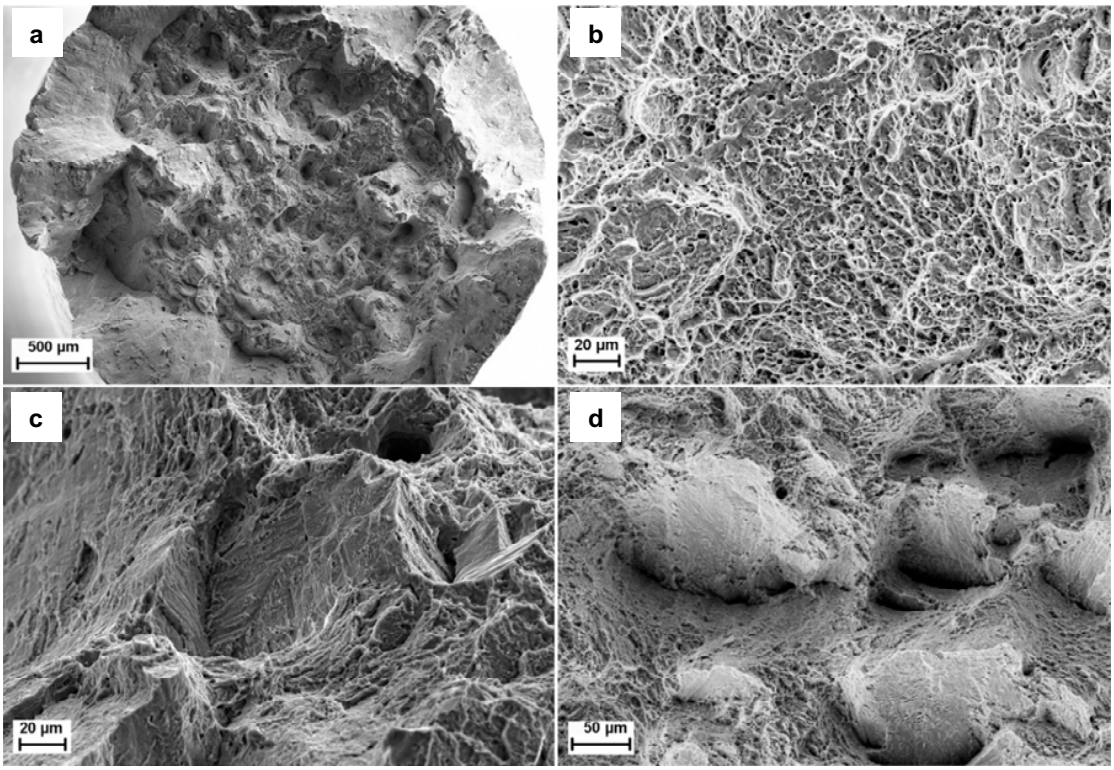

Fig. 2. Fractured surface: (a) cup-and-cone, (b) dimples, (c) and (d) quasi-cleavage facets in as-built SLM Ti6Al4V.

3.2. Tensile fracture mechanisms

The fracture surfaces after tensile tests of specimens in as-built and stress relieved conditions are similar in appearance. Typically, for ductile fracture, a cup-and-cone shape of the necking region was observed. The central area, commonly described as a region of fibrous fracture, was clearly distinguished apart from the shear lips on the periphery, Fig. 2(a). The fractured surface in the fibrous zone is quite irregular, not horizontal. Electron microscopy analysis revealed a formation of dimples, suggesting dimple rupture fracture in the fibrous zone, Fig. 2(b). On the surface of shear leaps, shallow dimples slightly elongated in the deformation direction were also visible.

The mechanisms of ductile fracture and the formation of a cup-and-cone shape in the necking region are usually associated with pore coalescence. Although the dimple rupture was dominating, some quasi-cleavage facets features of both ductile and brittle kind were observed, Figs. 2(c) and (d). High-magnification analysis showed that martensite needles are often visible on the quasi-cleavage surfaces. Therefore, it is possible to confirm that these regions are formed when the crack propagates along a martensite colony. When the crack reaches a primary β grain boundary, Fig. 2 (d), or a fusion boundary Fig. 2 (c), the growth direction is changed. The interface, therefore, acts as a crack deflector preventing quick failure. This conclusion is in agreement with results presented by Wen et al., (2014).

The presence of initial porosity in the SLM specimens and also its development under tension could also explain the irregular surface of the fibrous zone. A highly irregular fracture surface implies intensive crack deflection during tension, i.e. when the pores and the micro-voids coalesced, they formed not only horizontal but also inclined surfaces. This results in the formation of the quite irregular final surface observed in the fibrous zone. An additional reason for the irregularity of the fracture surface could be residual stresses locally affecting crack propagation. Since the same kind of irregular fracture surface was observed in both as-built and stress relieved specimens, this cannot be the case here.

3.3. Necking and development of pores under tension

In order to visualize and quantify the necking effect on the tensile samples, and estimate the reduction in area, the MicroCT was used in this study. The data was obtained according to a special procedure in which measured and reconstructed surface was compared with an ideal cylinder reference fitting the outer surface of the initial sample. In this way, the color-coded variance shows clearly the necking where red shows the largest variance, Fig. 3. It is seen that, volume involved in a formation of the neck differs in as-built and stress relieved SLM Ti6Al4V. It could be due to high residual stresses resulted different pore behavior and more pronounced localization of deformation in the as-built specimen.

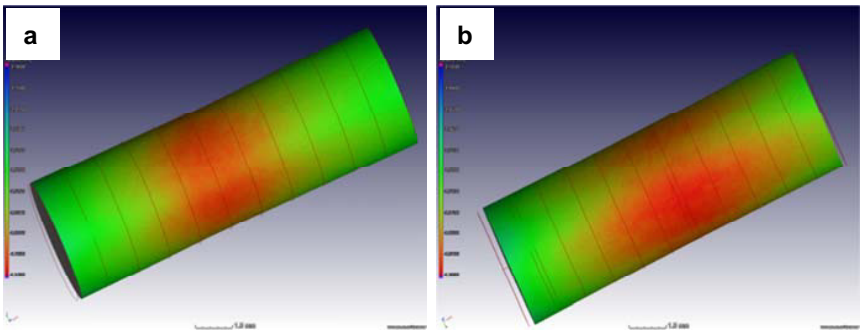

Fig. 3. Necking creation for (a) 8.25% pre-strained as-built sample; (b) 8.95% heat treated sample.

Development of porosity under deformation is essential new knowledge aimed to understand failure mechanisms and evaluate the deteriorating effect of porosity on the final tensile properties. For the analysis of pore deformation under load the computed tomography method was applied. This method has successfully been previously used in both in situ and ex situ setups (Buffierre et al., 2010). Very recently, a study of high resolution X-ray tomography of porosity and a shape of the necking region of micro tensile samples was reported by Benoit et al (2016) for commercially pure titanium and by Terzi et al (2009) for an aluminum alloy both manufactured in conventional way. In the current work, the ex situ changes in necking shape and porosity in standard tensile samples of 4-5 mm in diameter were analyzed. The analysis of porosity changes is new for this material and for this size of sample.

In this investigation, to observe the evolution of porosity, the development of pore size and morphology, and the influence of these parameters on mechanical behavior, several as-built and stress relieved specimens were pre-strained to 8.25 and 8.95% respectively. As the material was strained, pore coarsening was clearly pronounced and was dominating in the necking area, Fig. 4. The coalescence and growth of pores started in several different locations of the specimen. A comparison of pores before and after pre-strain, Figs. 1 and 4, clearly shows that morphology of the pores and their size were substantially changed. In the pre-strained as-built specimen, pores are coarser and look very much as agglomerates of several relatively round pores. The pores were interconnected with quite thin channels, possible cracks. In the stress relieved specimen similar trend was observed, although the crack regions were not so obviously pronounced. These observations, together with fracture surface analysis, confirm that pore growth and coalescence is the main crack formation mechanism.

These observations can also explain the big deviation among the experimentally observed values of elongation in the as-built SLM Ti6Al4V material, Table 1. If initial porosity is higher or pores are coarser, the pores grow and coalesce easier. This results in faster formation of the crack and final failure. Therefore, the difference in the initial porosity and pore morphology could remarkably influence the deviation in the final experimentally observed elongation. It is still unclear whether nucleation of new pores or growth, or coalescence of existing pores dominates the failure behavior. Therefore, further development of this approach including in situ computed tomography during deformation is required.

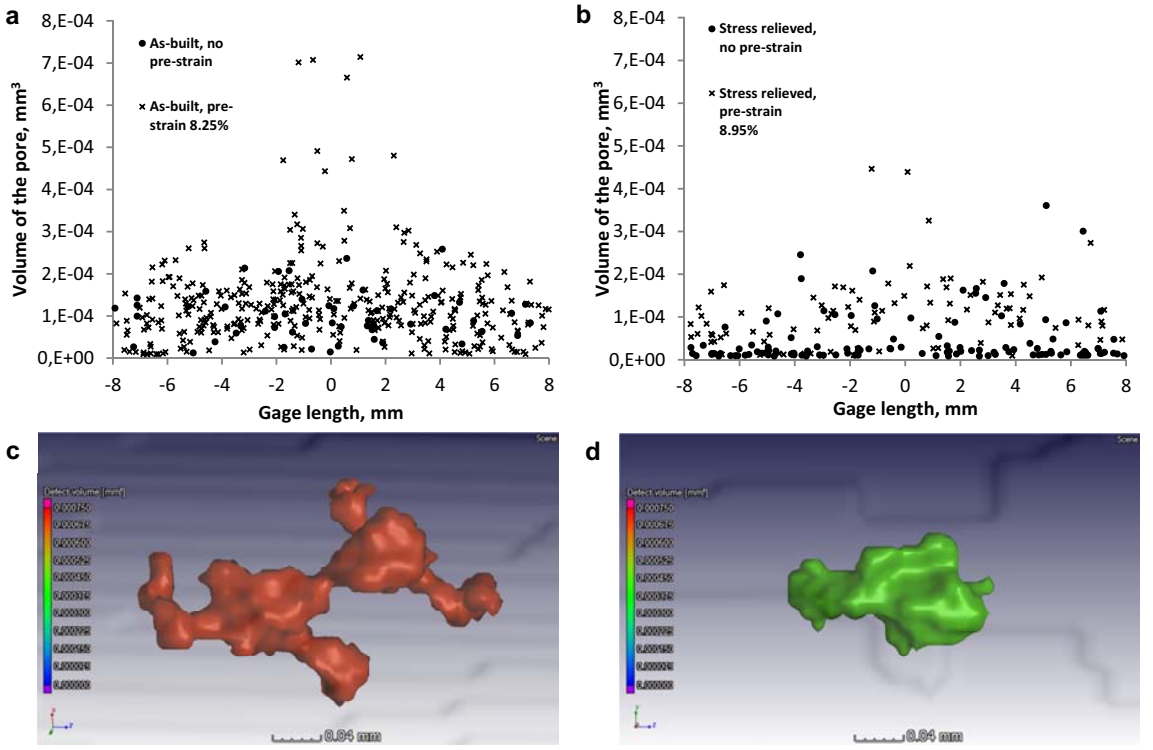

Fig. 4. Evolution of the pores in as-built (a, c) and stress-relieved (b, d) samples along tension direction.

3.4. Microstructure

At SLM, material solidifies with high cooling rates, which results in formation of metastable structures. In the case of Ti6Al4V, the microstructure after manufacturing typically consists of α′ martensite. Solidification of Ti6Al4V starts from crystallization of cubic β phase from the liquid. Commonly, cubic phase is crystallized with a preferential crystallographic direction <100>. Accordingly to Zhao et al. (2016) and Murr et al. (2009), further cooling leads to a transformation of β phase to α′ at high cooling rates (SLM), or α+β at lower cooling rates (EBM). In both cases, the newly formed hexagonal α phase has a crystallographic orientation relationship with parental β:

$$(110)_{bcc} \parallel (0001)_{hcp} \text{ and } \langle 1\bar{1}1\rangle_{bcc} \parallel \langle 11\bar{2}0\rangle_{hcp}$$

This type of crystallization texture has been confirmed by reconstruction of crystallographic texture in as solidified SLM and EBM Ti6Al4V by EBSD. Although β phase showed columnar growth with highly pronounced texture <100>, the texture of α′ was quite weak. It has been explained by a high number of variants that precipitate within each prior β grain (Simonelli et al., 2014). Generally, inner regions of the SLM object heat up and cool down

cyclically during manufacturing. It can result in initiation of diffusional processes and in situ decomposition of non-equilibrium phases. These processes were reported for instance by Xu et al. (2015) and Krakhmalev et al. (2015). Heat treatment in the α+β region also could lead to decomposition of the martensite. Sallica-Leva et al. (2016) and Simonelli et al. (2014) reported that decomposition of martensite started during stress relieve treatment.

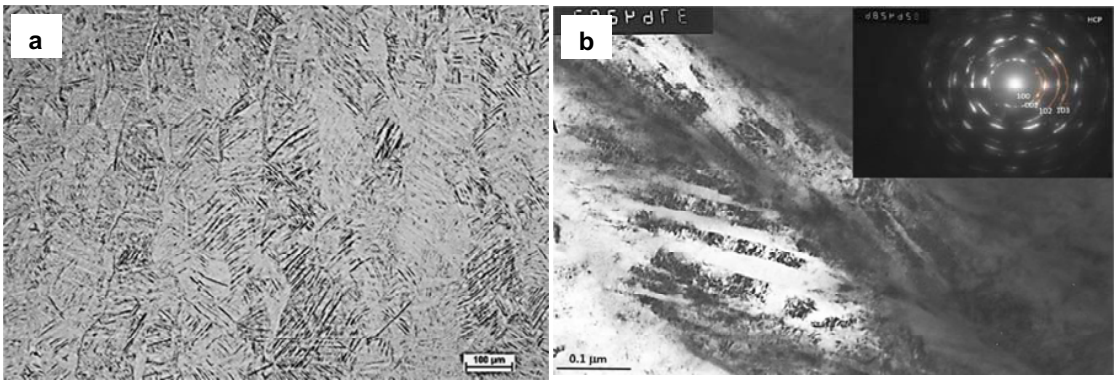

Fig. 5. Microstructure of SLM Ti6Al4V (ELI): (a) optical microscopy, columnar prior β grains oriented vertically along building direction, (b) TEM images of the microstructure after heat treatment, α´regions with thin twins. Ring SAED pattern taken with large aperture contained only α´ reflexes.

In the present research, investigations of specimens in as-built and stress relieved states observed a fully martensitic twinning structure. By XRD and TEM, no β (beta) phase was detected neither in as-built nor in stress relieved conditions. This indicates that β phase, if it exists in the material, is very fine, and/or is present in amounts below the detection limits of the used methods. Very fine acicular α´ martensite was also visible inside of the grain of prior β phase, Fig. 5 (b). It is known that compared to α (alpha) lamellae, α´ has slightly different lattice parameters, higher vanadium content and, commonly shows higher dislocation density, sometimes twins (Simonelli et al., 2012).

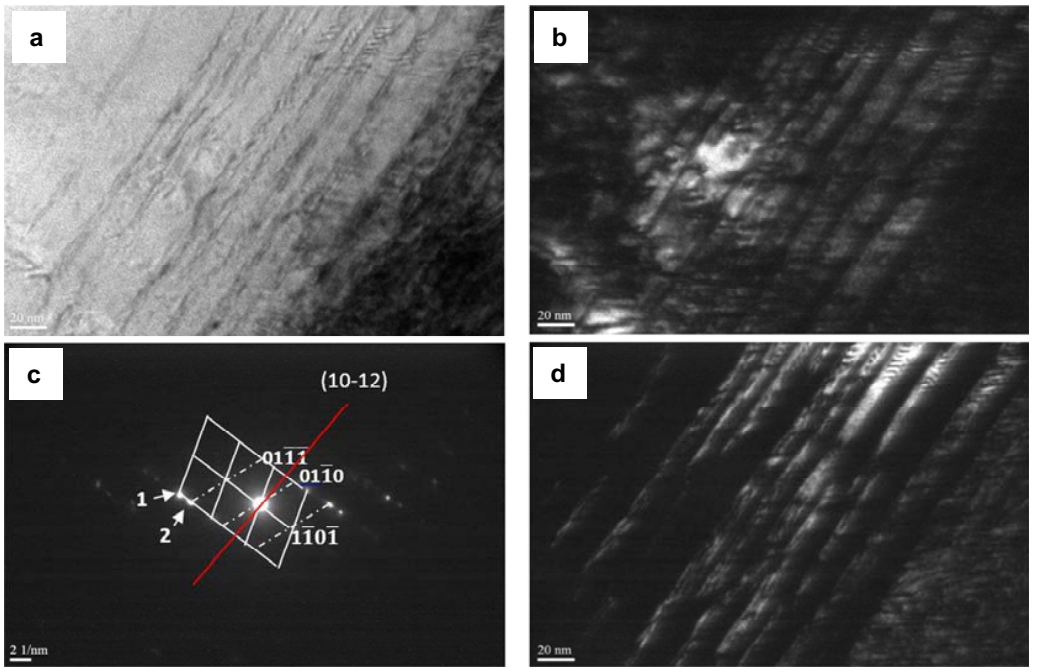

Fig. 6. TEM structure Ti6Al4V after SLM (initial), twins of *hcp* phase: (a)- the bright-field image; (b-c) the dark-field images in reflexes of $(2\bar{1}13)_m$ - (b) and $(1\bar{1}\bar{2}0)_t$ -(c); (d)- SAED pattern to (a-c), zone axis $[213\bar{1}]_m//[0001]_t$.

Since the critical resolved shear stress for activation of <*a*> basal slip is lower compared to other slip systems, twinning is not the dominating deformation mechanism in conventional Ti6Al4V (Zaefferer, 2003). In hexagonal metals, $\{10\bar{1}2\}$ $<\bar{1}011>$ and $\{11\bar{2}1\}$ $<\bar{1}\bar{1}26>$ tensile, and $\{11\bar{2}2\}$ $<11\bar{2}\bar{3}>$ and $\{10\bar{1}1\}$ $<10\bar{1}\bar{2}>$ compression twins were commonly observed (Britton et al., 2015).

In Ti6Al4V manufactured by additive manufacturing methods, twinning has been observed by Simonelli et al. (2012), Koike et al. (2011) and Murr et al. (2009). Nevertheless, a detailed examination and indexing of twinning in α′ martensite in SLM Ti6Al4V has not been presented. In this investigation, the type of twinning planes in the SLM Ti6Al4V was experimentally determined by TEM. Based on the selective area electron diffraction (SAED) data, all observed twins were of the same type, and they were identified as $\{10\bar{1}2\}$ twins. This type of twins in *hcp* materials is reported as tensile twins. In as-built specimens the α′ martensite appears as relatively long and narrow twin laths characterized by high dislocation density. SAED patterns taken from such twin regions reveal a high density of fringes and streaks indicating the possible presence of multiple stacking faults. The width of these twins was in the range of 10-15 nm, Fig. 6. The microstructure of the specimen after heat treatment was found similar to the microstructure of as-built one. The martensitic α′ phase also contained the *hcp* twins with a width of the twins about 25 nm.

Definition of twinning plane as $\{10\bar{1}2\}$ tensile twinning in the as-built material, which has never been conventionally plastically deformed, is a new and interesting result. This phenomenon could be explained if a thermomechanical history of the SLM material is taken into account. During manufacturing, surface heating and cooling affect the inner regions of the specimen. Due to high heating and cooling rates, thermal gradients are high and, therefore, thermal stresses also can reach quite high values. It commonly resulted in high tensile residual stresses observed on the top and in the volume of the laser manufactured objects (Yadroitsava et al., 2015). At SLM, high thermal stresses cyclically act on the inner regions, requiring activation of stress accommodation mechanisms. The observed twinning, therefore, is suggested as a possible mechanism for accommodation of cyclic thermomechanical stresses during manufacturing. The observed $\{10\bar{1}2\}$ twinning is classified as tensile and it

results in 16.7% strain in the <1000> direction in hexagonal close packed structure. Nevertheless, additional analysis are required to confirm tensile twinning as an in situ stress accommodation mechanism.

4. Conclusions

Microstructural analysis showed that fully martensitic α′structure with high dislocation density and stacking faults was typical in both the as-built and stress relieved samples. No β phase was detected by TEM and XRD.

Twinning was observed by means of TEM, and $\{10\bar{1}2\}$ twinning plane was defined in the as-built and stress relieved specimens. Twinning was suggested to be the mechanism for in situ accommodation of thermal stresses during manufacturing.

Pore coalescence was confirmed to be the main crack formation mechanisms in the final fracture with typical cup-and-cone fracture morphology. MicroCT analysis showed that average porosity did not exceed 0.0022 % (density >99.9). Pores were evenly distributed and mostly had an elongated shape. Pore coarsening and coalescence was observed in as-built and stress relieved specimens as they were pre-strained to 8.25 and 8.95 % respectively.

The ultimate tensile strength of 1265 MPa at a fracture strain of 9.4% was observed for the as-built material. After the heat treatment at 650°C during 3 h, strength decreased to 1170 MPa, while ductility increased to 10.9% that complies with the international standard for biomedical applications.

Acknowledgements

This work is based on the research supported by the South African Research Chairs Initiative of the Department of Science and Technology and National Research Foundation of South Africa (Grant №97994) and the Collaborative Program in Additive Manufacturing (Contract №CSIR-NLC-CPAM-15-MOA-CUT-01).

References

Beese, A.M., Carroll, B.E. 2016. Review of mechanical properties of Ti-6Al-4V made by laser-based additive manufacturing using powder feedstock. JOM 68, 724-734.

Benoit, R.B., Cazacu, O., Flater, P., Chandola, N. and Alves, J.L., 2016. Unusual plastic deformation and damage features in Titanium: experimental tests and constitutive modeling. Journal of the Mechanics and Physics of Solids.

Boyer, R., Welsch, G., Collings, E., 1994. Materials Properties Handbook: Titanium Alloys, Materials Park, Ohio: ASM International, Technology & Engineering.

Britton, T.B., Dunne, F.P.E., Wilkinson, A.J., 2015. On the mechanistic basis of deformation at the microscale in hexagonal close-packed metals. Proceeding of Royal Society A 471, 20140881.

Buffiere, J.Y., Maire, E., Adrien, J., Masse, J.P. and Boller, E., 2010. In situ experiments with X ray tomography: an attractive tool for experimental mechanics. Experimental mechanics, 50(3), pp.289-305.

Donachie, M.J., 2000. Titanium: A Technical Guide, 2nd Ed, Materials Park, Ohio: ASM International, Technology & Engineering.

du Plessis, A. and Rossouw, P., 2015. Investigation of porosity changes in cast Ti6Al4V rods after hot isostatic pressing. Journal of Materials Engineering and Performance, 24(8), pp.3137-3141.

Facchini, L., Magalini, E., Robotti, P., Molinari, A., Hoges, S., Wissenbach, K., 2010. Ductility of a Ti-6Al-4V alloy produced by selective laser melting of prealloyed powders. Rapid Prototyping Journal 16/6, 450–459.

Frey, M., Shellabear, M., Thorsson, L., 2009. Mechanical testing of DMLS parts. EOS whitepaper, EOS GmbH Electro Optical Systems, Munich.

Kasperovich, G., Hausmann, J., 2015. Improvement of fatigue resistance and ductility of TiAl6V4 processed by selective laser melting, Journal of Materials Processing Technology 220, 202–214.

Krakhmalev, P., Yadroitsava, I., Fredriksson, G., Yadroitsev, I., 2015. In situ heat treatment in selective laser melted martensitic AISI 420 stainless steels, Materials & Design 87, 380-385.

Koike, M., Greer, P., Owen, K., Lilly, G., Murr, L.E., Gaytan, S.M., Martinez, E., Okabe, T., 2011. Evaluation of Titanium Alloys Fabricated Using Rapid Prototyping Technologies-Electron Beam Melting and Laser Beam Melting. Materials 4, 1776-1792.

Maskery I., Aboulkhair N.T., Corfield M.R., Tuck C., Clare A.T., Leach R.K., Wildman R.D., Ashcroft I.A., Hague, R.J.M., 2016. Quantification and characterisation of porosity in selectively laser melted Al–Si10–Mg using X-ray computed tomography. Materials Characterization 111, 193-204.

Mertens, A., Reginster, S., Paydas, H., Contrepois, Q., Dormal, T., Lemaire, O., Lecomte-Beckers. J,. 2014. Mechanical properties of alloy Ti–6Al–4V and of stainless steel 316L processed by selective laser melting: influence of out-of-equilibrium microstructures. Powder Metallurgy 57(3), 184-189.

Miura, H., Itoh, Y., Ueamtsu, T., Sato, K., 2010. The influence of density and oxygen content on the mechanical properties of injection molded Ti-6Al-4V alloys. Advances in Powder Metallurgy and Particulate Materials 1, 46-53.

Murr, L.E., Quinones, S.A., Gaytan, S.M., Lopez, M.I., Rodela, A., Martinez, E.Y., Hernandez, D.H., Martinez, E., Medina, F., Wicker, R.B., 2009. Microstructure and mechanical behavior of Ti-6Al-4V produced by rapid-layer manufacturing, for biomedical applications. Journal of the Mechanical Behavior of Biomedical Materials 2, 20–32.

Rafi, H. N.V. Karthik, H. Gong, Th.L. Starr, and B. E. Stucker (2013). Microstructures and mechanical properties of Ti6Al4V parts fabricated by selective laser melting and electron beam melting. Journal of Materials Engineering and Performance 22, 3873–3883.

Sallica-Leva, E., Caram, R., Jardini, A.L., Fogagnolo, J.B., 2016. Ductility improvement due to martensite α′ decomposition in porous Ti–6Al–4V parts produced by selective laser melting for orthopedic implants. Journal of the Mechanical Behavior of Biomedical Materials 54, 149-158.

Sieniawski, J., Ziaja, W., Kubiak, K., and Motyka, M., 2013. Microstructure and Mechanical Properties of High Strength Two-Phase Alloys: Titanium Alloys - Advances in Properties Control, InTech, pp 69-80.

Simonelli, M., Tse, Y.Y., Tuck C.,2012. Further understanding of Ti-6Al-4V selective laser melting using texture analysis. Journal of Physics : Conference Series 371, 1-4.

Tammas-Williams, S., Zhaoa, H., Léonard, F., Derguti, F., Todd, I., Prangnell, P.B., 2015. XCT analysis of the influence of melt strategies on defect population in Ti–6Al–4V components manufactured by selective electron beam melting. Materials Characterization 102, 47–61.

Terzi, S., Salvo, L., Suéry, M., Limodin, N., Adrien, J., Maire, E., Pannier, Y., Bornert, M., Bernard, D., Felberbaum, M. and Rappaz, M., 2009. In situ X-ray tomography observation of inhomogeneous deformation in semi-solid aluminium alloys. Scripta Materialia, 61(5), pp.449-452.

Vilaro, T., Colin, C., Bartout J.D., 2011. As-fabricated and heat-treated microstructures of the Ti-6Al-4V alloy processed by selective laser melting. Metallurgical and materials transactions A 42, 3190-3199.

Vrancken, B., Cain, V., Knutsen, R. & Van Humbeeck, J., 2014. Residual stress via the contour method in compact tension specimens produced via selective laser melting. Scripta Materialia 87, 29–32.

Vrancken, B., Thijs, L., Kruth, J.P., Van Humbeeck, J., 2012. Heat treatment of Ti6Al4V produced by Selective Laser Melting . Journal of Alloys and Compounds 541, 177–185.

Wen, S., Li, S., Wei, Q., Yan, C., Zhang, S., Shi, Y., 2014. Effect of molten pool boundaries on the mechanical properties of selective laser melting parts. Journal of Materials Processing Technology 214, 2660-2667.

Xu, W., Brandt, M., Sun, S., Elambasseril, J., Liu, Q., Latham, K., Xia, K., Qian, M., 2015. Additive manufacturing of strong and ductile Ti–6Al–4V by selective laser melting via in situ martensite decomposition. Acta Materialia 85, 74–84.

Yadroitsev, I., Krakhmalev, P., Yadroitsava, I., 2014. Selective laser melting of Ti6Al4V alloy for biomedical applications: Temperature monitoring and microstructural evolution. Journal of Alloys and Compounds 583, 404-409.

Yadroitsava I., Grewar S., Hattingh D., Yadroitsev I., 2015. Residual stress in SLM Ti6Al4V alloy specimens, Materials Science Forum 828-829, 305-310.

Zaefferer, S., 2003. A study of active deformation systems in titanium alloys: dependence on alloy composition and correlation with deformation texture. Materials Science and Engineering A 344, 20-30.

Zhao, X., Li, S., Zhang. M., Liu. Y., Sercombe, T.B., Wang. S., Hao, Y., Yang, R., Murr, L.E., 2016. Comparison of the microstructures and mechanical properties of Ti–6Al–4V fabricated by selective laser melting and electron beam melting. Materials & Design 95, 21-31.

Ziółkowski, G., Chlebus, E., Szymczyk, P., Kurzac, J., 2014. Application of X-ray CT method for discontinuity and porosity detection in 316L stainless steel parts produced with SLM technology. Archives of Civil and Mechanical Engineering 14, 608-614.